Conference Proceedings

EuroSun 2016
Palma de Mallorca (Spain), 11 - 14 October 2016

Effect of the phase change material's melting point on the thermal behaviour of a concentrated photovoltaic system in a tropical dry climate

Jawad Sarwar[1], Brian Norton[2] and Konstantinos E. Kakosimos[1]

[1] Sustainable Energy and Clean Air Research Laboratory, Department of Chemical Engineering, Texas A&M University at Qatar, 23874, Doha, Qatar

[2] Dublin Energy Lab, Dublin Institute of Technology, Grangegorman, Dublin 7, Ireland

Abstract

In this work, we investigated temperature regulation of concentrating photovoltaic (CPV) and thermal energy storage using solid-liquid phase change material (PCM) under tropical dry climatic conditions. A finite element based heat transfer model is developed that includes the optical behavior of incident irradiance, solar to electrical conversion and online calculation of heat loss coefficients. The model's results are in good agreement (±3 ºC) against indoor experimental results. The validated model is used to predict the thermal behavior of PV and CPV incorporating PCM by varying melting point (35 ºC to 75 ºC), ambient temperature (30 ºC to 50 ºC) and concentration ratio (2× - 4×). It is found that a PCM with melting temperature in the range of 45 ºC to 65 ºC is suitable for temperature regulation and thermal energy storage for a CPV system in a tropical dry climate for up to ~ 4×. The choice of an appropriate PCM in melting temperature range of 45 ºC – 65 ºC depends on energy utilization requirement. The overall efficiency of the CPV system with a PCM makes it an attractive choice for a CPV thermal application in a tropical dry climate.

Keywords: *Phase change material, concentrated photovoltaic, finite element, heat transfer*

1. Introduction

Concentrating solar radiation onto photovoltaic (PV) cells generates more electricity but concomitantly raises the PV cell operating temperature thereby decreasing solar to electrical conversion efficiency by 0.08 %/K for crystalline silicon PV (Radziemska, 2003). Solid-liquid phase change material (PCM) is a promising technology to regulate the temperature of PV along with enabling thermal storage of energy (Hasan et al., 2015). A PCM stores energy during phase change otherwise acts as a sensible heat storage material. The absorption, storage and releasing capability of a PCM depends on its geometrical configuration and its thermophysical properties (Sarwar and Mansoor, 2016). A comprehensive review of integration of a PCM for thermal management of photovoltaic has shown that the PCM is not only useful for non-concentrating PV but has particular potential for temperature regulation of concentrated photovoltaic (CPV) application (Browne et al., 2015).

Recently, several researchers have experimentally and numerically investigated the performance enhancement of CPV using a PCM. For example, an in-door experimental investigation of a low concentrated, geometrical concentration ratio of 2.7, building integrated CPV containing a paraffin wax (RT42) has been carried out. It is reported that the PCM effectiveness depends upon the incident irradiance intensity and the integration of PCM reduces module center temperature by an average of 3.8 ºC (Sharma et al., 2016). An outdoor investigation of another low concentrated CPV system integrated with a paraffin wax (melting temperature of 47 ºC) has shown a decrease in PV temperature and increase in solar to electrical conversion efficiency (Ceylan et al., 2016). A theoretical investigation of application of a PCM in a photovoltaic-thermoelectric system has

doi:10.18086/eurosun.2016.08.12 Available at http://proceedings.ises.org

been undertaken to determine PCM influence on electrical conversion (Cui et al., 2016). The results are compared with a photovoltaic-thermoelectric system without a PCM. It is reported that introduction of a PCM increases the electrical conversion efficiency and mitigates the temperature fluctuations of a PV cell. It is also discussed that the selection of an appropriate PCM depends on desired operating temperature conditions (Cui et al., 2016). A combination of heat spreading and PCM cooling method has been employed to experimentally investigate the temperature regulation of a PV cell under concentrated irradiance (optical concentration ratio of 4). It is reported that the introduction of PCM (Fatty acids and salt hydrates) reduces the peak PV cell temperature in the range of 9 ^{o}C – 20 ^{o}C (Sarwar et al., 2013). An indoor and outdoor investigation of a CPV using a V-trough as a concentrator and a PCM having melting temperature of 57 ^{o}C has also reported the temperature regulation ability of the PCM (Maiti et al., 2011).

Although, temperature controlling ability of a PCM is well established but selection of an appropriate PCM is critical to design an efficient system that can work over the whole year. The PCM used should have a large latent heat of fusion, reversible phase change and melting point within a range of operation (Cabeza et al., 2011). On the other hand, ambient conditions play an equally important role in selection of a PCM in extreme conditions such as a tropical dry climate (i.e. Qatar, Middle East). Nocturnal ambient or radiative cooling temperatures must fall below the melting temperature to solidify the PCM for operation the next day. A multi-year (1978-2012) analysis of the weather data for Qatar showed that during summer night, temperature can go as high as up to 32 ^{o}C while peak temperature during summer day can reach up to 50 ^{o}C. In this preliminary analysis we considered the effect of ambient temperature (e.g. no humidity) and melting temperature. Therefore, we consider PCMs with a melting point in the range of 35 - 75 ^{o}C for the temperature regulation and calculate the electrical and thermal energy storage performance of selected system. The ambient temperature is considered in the range of 30 - 50 ^{o}C while the concentrated flux intensity is considered up to 4 kWm^{-2}.

2. Optical-thermal model

A finite element based heat transfer model is coupled with an optical model to evaluate the thermal, optical and electrical behavior of a photovoltaic cell integrated with a phase change material. The schematic illustration of different physical phenomena within the system is shown in Fig. 1.

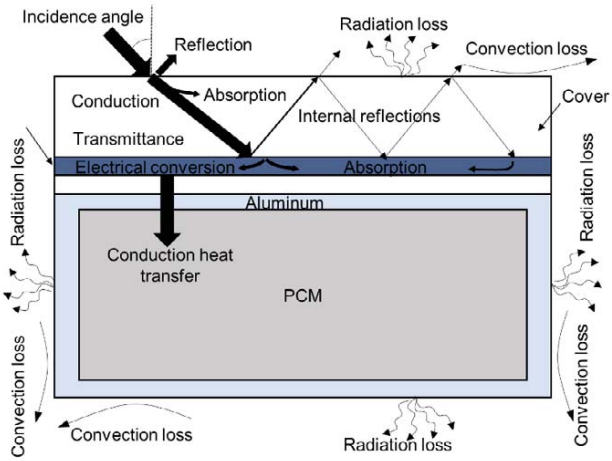

Fig 1: Physical phenomena within the photovoltaic/phase change material system

The principles of the optical-thermal model are as follows:

- A 2D differential heat diffusion equation is used to develop the finite element based heat transfer model. The weak formulation is developed using a test function and integrating it over the domain and its boundary. Green-Gauss theorem and divergence theorem are used to simplify the formulation. An 8-node Serendipity element is used to transform physical coordinates to natural coordinates. The elements are assembled using direct addition of components method to form the domain of the system.

- Latent heat of fusion effect is introduced via an effective heat capacity method.
- The temporal discretization is carried out using a Crank-Nicholson method.
- Convection and radiation losses are considered on all sides of the system.
- Reflectance, transmittance and absorptance is calculated using Fresnel equations method.
- Angle of incidence of sun's irradiance is found via a methodology proposed by Hoang et al. (2014).
- Temperature dependence of electrical conversion is considered for calculations of electrical power generation by incident irradiance.

The following assumptions are made to simplify the calculations:

- Multiple reflections up to 3 are considered in the cover.
- Incident diffuse and direct radiations are considered un-polarized.
- Effective thermal conductivity of the PV cell is used instead of using thermal conductivity of each layer of the PV cell.
- Only conduction heat transfer in the PCM is considered.

2.1 Thermal model

A two-dimensional differential heat diffusion equation governing transient heat transfer in the system shown in Fig. 1 is as follows:

$$\rho c \frac{\partial T}{\partial t} - \left[\frac{\partial}{\partial x_i}\left(k_{ij}\frac{\partial T}{\partial x_j}\right)\right] = 0 \qquad \text{(eq. 1)}$$

The convection and radiation heat losses at the boundary of the system are given by following equations:

$$H = h_c A \Delta T \qquad \text{(eq. 2)}$$

$$R = h_r A \Delta T \qquad \text{(eq. 3)}$$

The energy balance of the system is obtained using equation eq. 1 – eq. 3 and multiplied by a test function δT and integrated over the domain to get its weak formulation. The Green-Gauss theorem and divergence theorem is applied on the relevant equations to obtain simplified form of the weak formulation which is given as:

$$\int_\Omega \delta T \rho c \frac{\partial T}{\partial t} \partial\Omega + \int_\Omega \left[k_{11}\frac{\partial \delta T}{\partial x_1}\left(\frac{\partial T}{\partial x_1}\right) + k_{22}\frac{\partial \delta T}{\partial x_2}\left(\frac{\partial T}{\partial 2}\right)\right]\partial\Omega - \int_\Gamma \delta T q \partial A + \int_\Gamma \delta T (H+R)\partial A = 0 \qquad \text{(eq. 4)}$$

The differential of temperature and test functions are transformed from physical coordinates into natural coordinates by using chain rule and an 8-node Serendipity element. After transformations, the energy balance equation becomes as:

$$\mathbf{M}\dot{T} + \mathbf{K}T - \boldsymbol{q} + (\mathbf{H}+\mathbf{R})T = 0 \qquad \text{(eq. 5)}$$

where $\dot{T}$ is the time derivate of temperature while **M**, **K**, **H**, **R** and $\boldsymbol{q}$ are the mass, conductivity, convection, radiation and irradiance matrices. These matrices are calculated as:

$$\mathbf{M} = \int_{-1}^{1}\int_{-1}^{1} \rho c N^T N |J| h \partial\xi_1 \partial\xi_2 \qquad \text{(eq. 6)}$$

$$\mathbf{K} = \int_{-1}^{1}\int_{-1}^{1} B^T k B |J| h \partial\xi_1 \partial\xi_2 \qquad \text{(eq. 7)}$$

$$\mathbf{H} = \int_{-1}^{1} h_c N^T N |J_i| h \partial\xi_{1\ or\ 2} \qquad \text{(eq. 8)}$$

$$\mathbf{R} = \int_{-1}^{1} h_r N^T N |J_i| h \partial\xi_{1\ or\ 2} \qquad \text{(eq. 9)}$$

$$\mathbf{q} = \int_{-1}^{1} q N^T N |J_i| h \partial\xi_{1\ or\ 2} \qquad \text{(eq. 10)}$$

N represents an 8-node Serendipity element, B is the B-operator, ξ is the natural coordinates, J is Jacobian matrix and h is the width of the system. The physical discretization of the domain is obtained by assembling

the elements using direct addition of components method. The temporal discretization of the system is carried out using a Crack-Nicholson scheme. The convection and radiation heat transfer coefficients are calculated at each time step using following equations:

$$h_c = 2.9v + 4.5 \quad \text{(eq. 11)}$$

$$h_r = \sigma \varepsilon F \left(\frac{T^4 - T_a^4}{T - T_a}\right) \quad \text{(eq. 12)}$$

Where v is the velocity of the air, σ is the Stefan-Boltzmann constant, ε is the emissivity and T_a is the ambient temperature. In current calculations, the ambient temperature is considered equal to the sky temperature (Kumar and Mullick, 2012) and view factor is considered as 1. For indoor calculations, velocity of the air is considered as zero. The latent heat effect of the PCM is introduced using an effective heat capacity method (Lamberg et al., 2004) which is as follows:

$$c_e = \begin{cases} c_s & T < T_1 \\ c_s + \frac{L}{T_2 - T_1} & T_1 \le T \le T_2 \\ c_l & T > T_2 \end{cases} \quad \text{(eq. 13)}$$

Where c_e is the effective heat capacity of the PCM, c_s and c_l are the heat capacities of solid and liquid PCM respectively. L is latent heat of fusion while T_1 and T_2 are the melting onset and solidification temperature respectively.

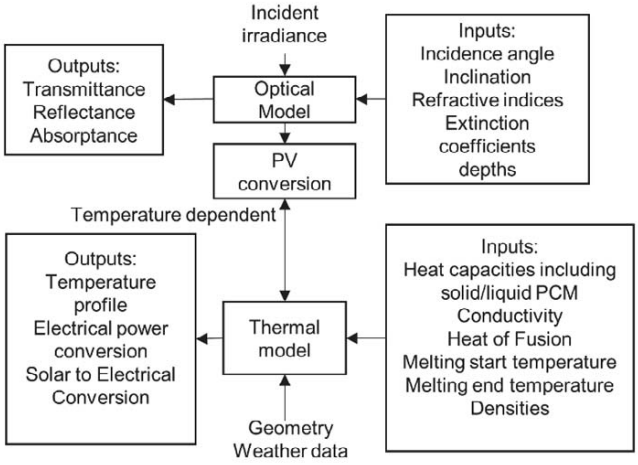

Fig. 2: Flow chart representation of the optical-thermal model

2.2 Optical model

The irradiance incident on the PV cover goes through the series of reflections and absorptions in the cover, as shown in Fig. 1, before absorbing in the PV cell. The reflectance, absorptance and transmittance in the system is calculated using Fresnel equations (Hecht, 2002).

$$\begin{aligned} &\rho = \tfrac{1}{2}(\rho_\parallel + \rho_\perp) \quad \rho_\perp = -\frac{sin(\theta_i - \theta_t)}{sin(\theta_i + \theta_t)} \quad \rho_\parallel = \frac{tan(\theta_i - \theta_t)}{tan(\theta_i + \theta_t)} \\ &\tau = \tfrac{1}{2}(\tau_\parallel + \tau_\perp) \quad \tau_\perp = \tau_a \left(\frac{1-\rho_\perp}{1+\rho_\perp}\right)\left(\frac{1-\rho_1^2}{1+\rho_1^2\tau_a^2}\right) \quad \tau_\parallel = \tau_a \left(\frac{1-\rho_\parallel}{1+\rho_\parallel}\right)\left(\frac{1-\rho_\parallel^2}{1+\rho_\parallel^2\tau_a^2}\right) \\ &\alpha = \tfrac{1}{2}(\alpha_\parallel + \alpha_\perp) \quad \alpha_\perp = (1-\tau_a)\left(\frac{1-\rho_\perp}{1+\rho_\perp\tau_a}\right) \quad \alpha_\perp = (1-\tau_a)\left(\frac{1-\rho_\perp}{1+\rho_\perp\tau_a}\right) \\ &\tau_a = e^{\frac{-Kx}{cos\theta_t}} \end{aligned} \quad \text{(eq. 14)}$$

A transmittance angle (θ_t) is calculated from an incident angle (θ_i) by using Snell's refractive law. For indoor calculations, the incident irradiance is assumed normal to the cover but for the outdoor calculations, the incident angle is found using a methodology available in literature (Hoang et al., 2014). The formulae for

calculations of incidence angle, sun declination angle (δ) and hour angle (ω) are presented in eq. 15.

$$\cos\theta_i = \sin\delta \times \sin l \times \cos s - \sin\delta \times \cos l \times \sin s \times \cos\varphi + \cos\delta \times \cos l \times \cos s \times \cos\omega + \cos\delta \times \sin l \times \sin s \times \cos\varphi \times \cos\omega + \cos\delta \times \sin s \times \sin\varphi \times \sin\omega$$
$$\delta = 0.38 + 23.26 \sin\left(\frac{2\pi J'}{365.24-1.395}\right) + 0.37 \sin\left(\frac{4\pi J'}{365.24-1.457}\right) \quad \text{(eq. 15)}$$
$$\omega = 15 \times \left(H_l - \Delta H_l + \Delta H_g - E - 12\right)$$
$$E = 7.5 \times \sin\left(2\pi \frac{J'}{365.24} - 0.03\right) + 0.99 \times \sin\left(4\pi \frac{J}{365.24} + 0.35\right)$$

Where J' is the rank of the day after the first of January 2013 while J is the Julian day of the year. The local time is represented by H_l, time lag between the given time zone and UTC is represented by ΔH_l and time lag due to the longitude variation is denoted by ΔH_g.

2.3 Coupling of optical-thermal model

The flow chart representation of the optical-thermal model is shown in Fig. 2. The irradiance available at the PV after going through series of reflections and absorption losses in the PV cover is obtained via following equation:

$$q_{aol} = (1 - \rho - \alpha) q_i \quad \text{(eq. 16)}$$

The part of the irradiance available at the PV is converted in to electricity while rest is converted in to heat. The irradiance after accounting for electrical conversion is shown in equation 17.

$$q = q_{aol} - [\eta + \mu(T - T_a)] q_{aol} \quad \text{(eq. 17)}$$

Where η is the efficiency and μ is the power output temperature coefficient of the PV cell under standard test conditions.

The irradiance (q) is updated at every time step to include temperature dependence properties of the PV cell and incidence angle variations over the day. The electrical power produced from the PV cell is calculated using following correlation:

$$P = q_{aol}\, A\, \eta\, [1 - \mu(T - 298)] \quad \text{(eq. 18)}$$

Furthermore, the thermal efficiency of the CPVPCM system is calculated by calculating the ratio of thermal energy stored in the PCM (Hasan et al., 2015) to the incident energy.

2.4 Input parameters of the optical-thermal model

The electrical, thermal and optical properties of the materials that serve as an input in the optical-thermal model are presented in table 1.

Tab. 1: Thermal parameters of the materials used in the system for the optical-thermal model

	Thermal parameters of the materials					
	ρ (kg m^{-3})	k ($Wm^{-1}K^{-1}$)	c ($kJkg^{-1}K^{-1}$)	ε	H ($kJkg^{-1}$)	T_m (K)
Perspex	1190	1.9	1.3	0.9	×	×
PV	2205	125.4	0.8	0.9	×	×
Aluminium	2700	205.0	0.9	×	×	×
PCM	880	0.2	1.3 (s) 1.8 (l)	×	190	303 - 323
	Electrical characteristics					
	η			μ ($^oC^{-1}$)		
	12.7			-0.005		
	Optical parameters of the materials					
	n		K (m^{-1})		x (m)	
Perspex	1.5		10		3×10^{-3}	
PV	4		4710		5×10^{-4}	

A clear sky broadband solar radiation model (Bird and Hulstrom, 1981) is used to simulate the direct beam and global horizontal irradiance. The latitude and longitude of the selected location (Education city, Doha, Qatar) are 25.314779° N and 51.43978° E respectively. Four days (January 1, March 30, June 29 and September 29) belonging to each season of a year 2015 are selected to predict the electrical, thermal and optical behaviour of the selected system. The weather data including wind speed and ambient temperature for the selected days is obtained from experimentally measured data by meteorological department, Qatar. The variations in irradiance, ambient temperature and wind speed on selected days are shown in Fig. 3. Thermal and electrical output of the system under concentrated irradiance, referred as CPVPCM in subsequent text, is predicted and compared with non-concentrated PV. The inclination angle of the PV for non-concentrated system is considered equal to the latitude of the location while dual-axes tracking is considered for CPVPCM system with an error of ±0.1°.

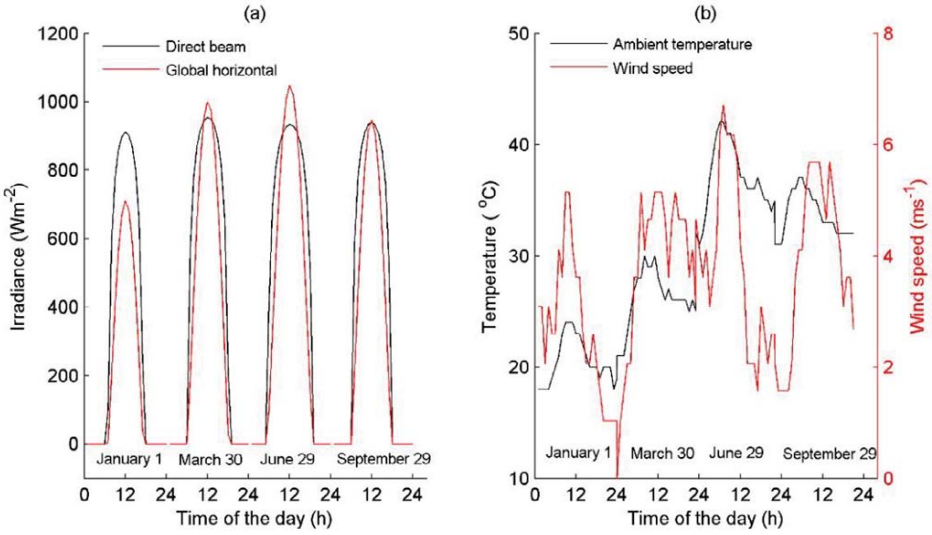

Fig. 3: The irradiance, ambient temperature and wind speed variations on selected days

3. Experimental setup and model validation

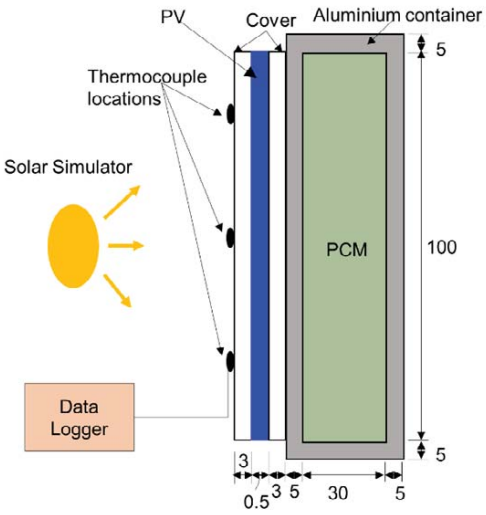

Fig. 4: Schematic illustration of the experimental setup

The schematic illustration of experimental setup is shown in Fig. 4. Polycrystalline silicon PV cell, Suntech power STP065-12/Sb, (Solar, 2013) with the dimensions of 100 mm × 100 mm × 0.5 mm encapsulated in a 3 mm thick Perspex imitated the PV cell. The volume of PCM required for temperature regulation of the PV cell, was calculated using an energy balance equation presented by Huang et al. (Huang et al., 2004) by

considering RT20 as a PCM. A 5 mm thick aluminium sheet was used to fabricate a 30 mm thick aluminium container encapsulating a PCM having a volume of 0.3 litres. Five T-type copper-constantan thermocouples with a maximum measurement deviation of ±0.2 °C were attached to the front surface of the system to measure the temperature at a sampling rate of 100 Hz using a data logger. The system is irradiated at 1000 Wm^{-2} using a Griven GR262 solar simulator and the flux is measured using a Kipp & Zonen CM6B pyranometer. The height of the solar simulator and PV cell was adjusted to keep the irradiance normal to the centre of the PV cell. The experiments were performed three times to ensure repeatability and to quantify the uncertainty in the experimental results. The average of the measured experimental PV cell temperature along with error bars depicting uncertainty was compared with numerically predicted temperature under same irradiance to validate the numerical model.

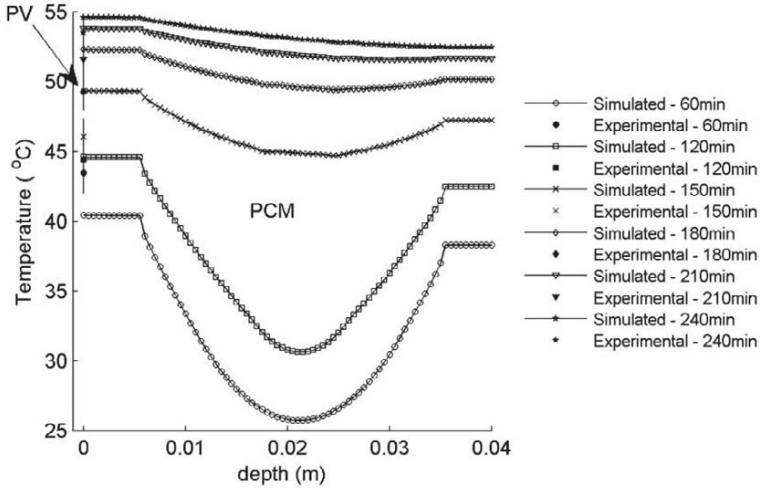

Fig. 5: Comparison of experimental and numerical temperature along with melting behavior of a phase change material

It is shown in figure 5 that the temperature of the PV cell is in agreement with numerically predicted temperature. The experimental temperature of the PV cell increases to 43.4 °C in one hour while it increases to 53.9 °C while exposed to 1000 Wm^{-2} for four hours. The corresponding numerical temperatures are 41 °C and 54.6 °C respectively. A maximum standard deviation of ±3 °C is achieved between experimental and numerical temperatures thereby, validating the optical-thermal model. The melting behavior of the system is also shown in Fig. 5 which indicates that heat is transferred to the PCM from both front and back side. Although irradiance is incident on the PV cell only but heat is transmitted to the back of the container fast through the aluminum containment due to its high thermal conductivity. Therefore, the melting of the PCM starts from each side of the container and completes in the center of the container.

4. Results and Discussion

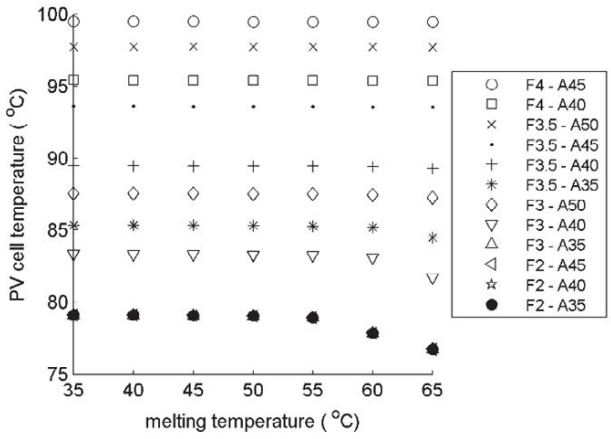

Fig. 6: Temperature of the CPVPCM system under variable concentrated irradiance, ambient and melting temperature

The temperature of the CPVPCM system under in-door conditions has been investigated using developed optical-thermal model for variable incident concentrated irradiance up to 4 kWm^{-2}. The ambient temperature has been varied in the range of 35 ^oC – 50 ^oC while melting temperatures of the PCM are varied in the step of 5 ^oC from 35 ^oC to 65 ^oC. The result is shown in Fig. 6.

The temperature of the PV cell increases with the increase in ambient temperature and increase in concentrated irradiance. The PV cell temperature decrease with the increase in the melting temperature but the difference is more pronounced at lower concentrated irradiance up to 3 kWm^{-2}. The temperature of the PV cell in the CPVPCM system can be maintained below 85 ^oC up to concentrated irradiance of 3.5 kWm^{-2} under indoor conditions. To investigate the electrical and thermal behavior of the CPVPCM system under out door conditions, the temperature evolution and electrical output of the system is simulated for PCM melting temperatures of 45 ^oC and 65 ^oC. The simulated irradiance, ambient temperature and wind conditions, as shown in Fig. 3, of selected days of a year 2015 are used for that purpose. The incident concentrated and non-concentrated irradiance on the CPVPCM system and PV only after optical losses is shown in Fig. 7(a) while corresponding temperature evolution is shown in Fig. 7(b).

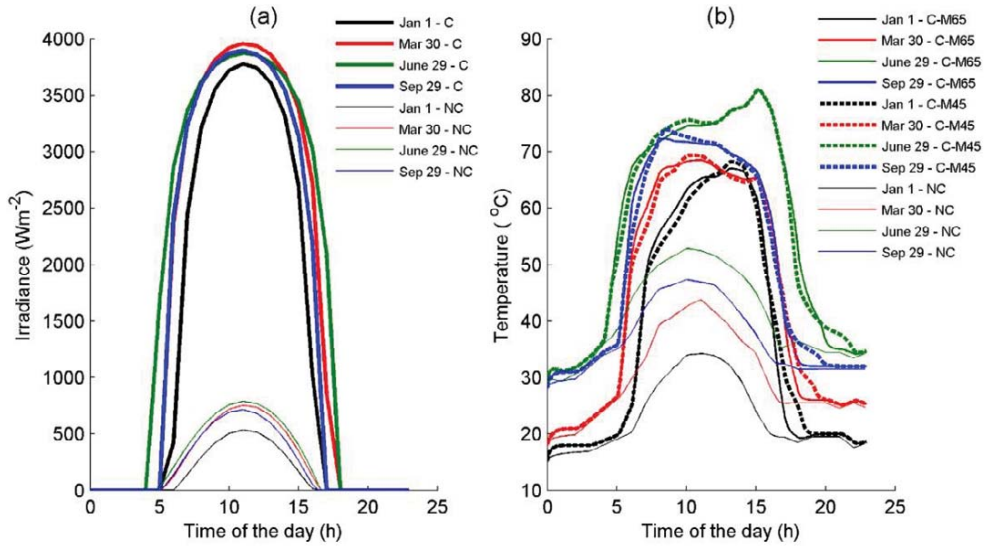

Fig 7: (a) Concentrated and non-concentrated irradiance after optical losses (b) Temperature evolution of the selected system and PV only

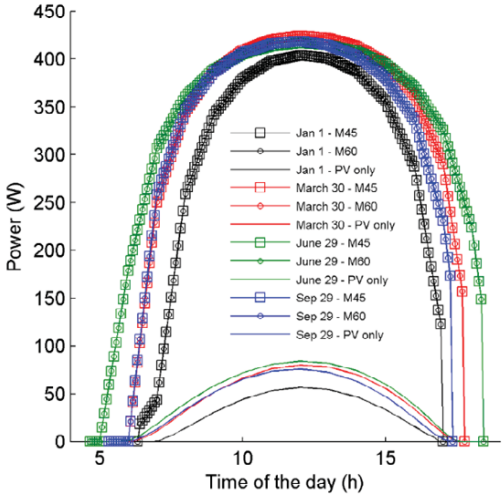

Fig 8: Electrical output of the system and PV only for a unit cell area

The peak concentrated irradiance varies in the range of 3.7 kWm^{-2} – 3.9 kWm^{-2} while non-concentrated irradiance varies in the range of 534 Wm^{-2} – 787 Wm^{-2}. The peak temperature of ~81 ^oC for the CPVPCM system is found in June while minimum peak temperature of ~68 ^oC is found in January. The change in melting

temperature of the PCM results in slight temperature increase of ~2 ºC for the melting temperature of 45 ºC. The peak temperature of PV only system varies in the range of 35 ºC – 53 ºC for selected days of the year. The hourly averaged incident irradiance and ambient temperature are used in the current investigations and the peak hourly average ambient temperature is ~ 40 ºC in June. The difference between peak PV temperature for PV only system and ambient temperature is ~ 13 ºC for incident irradiance of 787 Wm^{-2}. This difference is reasonable compared to a previous outdoor simulated analysis carried out by author, where the temperature difference between ambient to PV cell is obtained as 22 ºC for peak incident irradiance of ~ 980 Wm^{-2} (Hasan et al., 2015). There is a peak shifting in the temperature of the PV cell in the CPVPCM system is observed which is due to the integration of the PCM. This behavior is also consistent with previously reported experimental and simulated results (Hasan et al., 2015). The electrical output of both systems is investigated using equation 18 and result of electrical output is shown in Fig. 8. It is found that the electrical output of the system integrated with PCM remains almost same. The peak output of 424 W is obtained in March while peak output of 84 W is obtained for PV only system in June. The electrical output of the concentrated systems increases disproportionally with the increase in the incident irradiance. The incident irradiance increases by ~ 7 times but corresponding increment in electrical output is just ~5 times which is due to the temperature effect of the PV cell. Nevertheless, in current configuration, the electrical output remains unchanged by changing melting temperature from 45 ºC to 60 ºC but thermal behavior changes with the change in melting temperature of the PCM as shown in Fig. 9.

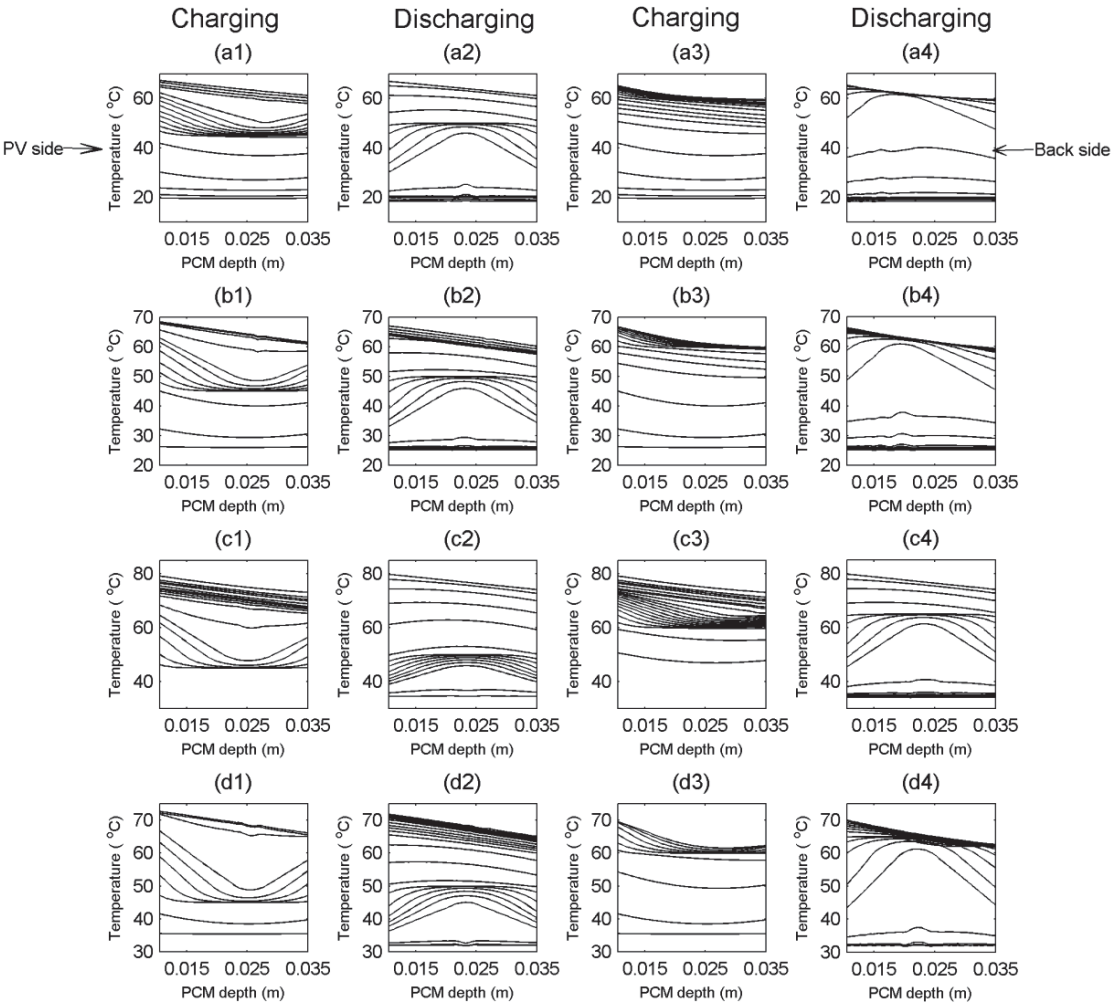

Fig. 9: Temperature curves in the PCM for every 30 minutes during charging and discharging (a) January 1 (b) March 30

(c) June 29 (d) September 29

The thermal energy storage in the PCM takes place at the melting temperature of the PCM as shown in Fig. 9. For the PCM, having melting temperature of 45 ºC, the temperature curves in the PCM shows energy storage and an extended temperature maintenance in the melting temperature range of 45 ºC – 50 ºC. The similar behavior is shown in Fig. 9 for the PCM having melting temperature of 65 ºC. This result shows that the PCMs having melting temperatures in between 45 ºC to 65 ºC are suitable for temperature regulation of a CPVPCM system. Thus, the selection of a PCM, in current configuration, also depends upon energy utilization requirement of the system. For example, if stored energy is required to be extracted at 45 ºC than PCM with a melting temperature of 45 ºC is appropriate and so on. The results of the electrical and thermal efficiencies of the systems are shown in Fig. 10.

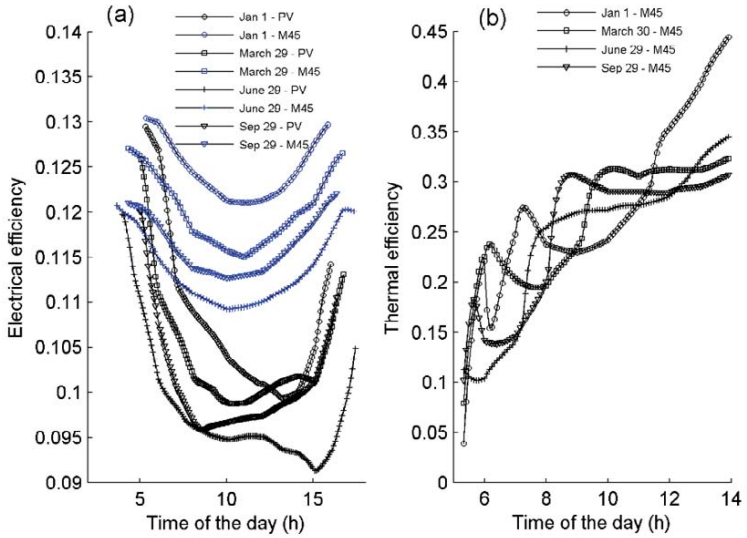

Fig. 10: (a) Electrical efficiency of the PV only and the system having PCM (b) thermal efficiency of the system

Despite increase in electrical power output for a unit area of CPVPCM system as compared to PV cell (as shown in Fig. 8), the overall electrical efficiency of the CPVPCM system decrease by ~16.5% than the PV system. But, the storage of thermal energy provides an advantage for the CPVCPM system and its thermal efficiency is found up to 45% during charging (Fig. 10). Therefore, the overall efficiency of the CPVPCM system is higher than the PV only system that makes it an attractive choice for a hybrid concentrated photovoltaic thermal application. Further studies are required to investigate the combined effect of other parameters of the CPVPCM system such as thermophysical properties of PCMs, geometry, containment thickness etc.

5. Conclusions

Following conclusions can be drawn from this work:

1. Developed optical-thermal model is a suitable tool for optical, thermal and electrical behavior of the system.
2. Ambient temperature and concentrated irradiance intensity effects the selection of a suitable PCM. A PCM with melting temperature in the range of 45 ºC to 65 ºC is suitable for temperature regulation and thermal energy storage for a CPV system in a tropical dry climate.
3. The utilization of stored energy from a PCM is another criterion for the selection of a PCM under limiting ambient and concentrated irradiance conditions.
4. The overall efficiency of a CPV system integrated with a PCM makes it an attractive alternative to a conventional PV system.

Acknowledgements

This publication was made possible by a PDRA award [PDRA2-1105-14044] from the Qatar National Research Fund (a member of The Qatar Foundation). The statements made herein are solely the responsibility of the authors. The HPC resources and services used in this work were provided by the IT Research Computing group in Texas A&M University at Qatar. IT Research Computing is funded by the Qatar Foundation for Education, Science and Community Development (http://www.qf.org.qa).

References

Bird, R. E. and R. L. Hulstrom (1981). Simplified clear sky model for direct and diffuse insolation on horizontal surfaces, ; Solar Energy Research Inst., Golden, CO (USA)**:** pp. Medium: ED; Size: Pages: 46. (1981).

Browne, M. C., B. Norton and S. J. McCormack (2015). "Phase change materials for photovoltaic thermal management." Renewable and Sustainable Energy Reviews **47**: 762-782.

Cabeza, L. F., A. Castell, C. Barreneche, A. de Gracia and A. I. Fernández (2011). "Materials used as PCM in thermal energy storage in buildings: A review." Renewable and Sustainable Energy Reviews **15**(3): 1675-1695.

Ceylan, İ., A. E. Gürel, A. Ergün and A. Tabak (2016). "Performance analysis of a concentrated photovoltaic and thermal system." Solar Energy **129**: 217-223.

Cui, T., Y. Xuan and Q. Li (2016). "Design of a novel concentrating photovoltaic–thermoelectric system incorporated with phase change materials." Energy Conversion and Management **112**: 49-60.

Hasan, A., S. J. McCormack, M. J. Huang, J. Sarwar and B. Norton (2015). "Increased photovoltaic performance through temperature regulation by phase change materials: Materials comparison in different climates." Solar Energy **115**: 264-276.

Hecht, E. (2002). Optics. San Francisco [etc.], Addison Wesley.

Hoang, P., V. Bourdin, Q. Liu, G. Caruso and V. Archambault (2014). "Coupling optical and thermal models to accurately predict PV panel electricity production." Solar Energy Materials and Solar Cells **125**: 325-338.

Huang, M. J., P. C. Eames and B. Norton (2004). "Thermal regulation of building-integrated photovoltaics using phase change materials." International Journal of Heat and Mass Transfer **47**(12-13): 2715-2733.

Kumar, S. and S. C. Mullick (2012). "Glass cover temperature and top heat loss coefficient of a single glazed flat plate collector with nearly vertical configuration." Ain Shams Engineering Journal **3**(3): 299-304.

Lamberg, P., R. Lehtiniemi and A.-M. Henell (2004). "Numerical and experimental investigation of melting and freezing processes in phase change material storage." International Journal of Thermal Sciences **43**(3): 277-287.

Maiti, S., S. Banerjee, K. Vyas, P. Patel and P. K. Ghosh (2011). "Self regulation of photovoltaic module temperature in V-trough using a metal–wax composite phase change matrix." Solar Energy **85**(9): 1805-1816.

Radziemska, E. (2003). "The effect of temperature on the power drop in crystalline silicon solar cells." Renewable Energy **28**(1): 1-12.

Sarwar, J., M. Browne, S. McCormack, M. J. Huang and B. Norton (2013). Experimental investigation of temperature regulation of concentrated photovoltaic using heat spreading and phase change material cooling method. The 2nd International Conference on Sustainable Energy Storage (IC-SES), Dublin, Ireland.

Sarwar, J. and B. Mansoor (2016). "Characterization of thermophysical properties of phase change materials for non-membrane based indirect solar desalination application." Energy Conversion and Management **120**: 247-256.

Sharma, S., A. Tahir, K. S. Reddy and T. K. Mallick (2016). "Performance enhancement of a Building-Integrated Concentrating Photovoltaic system using phase change material." Solar Energy Materials and Solar Cells **149**: 29-39.

Solar, I. (2013). "Solar modules - polycrystalline, Suntech power STP040-12/Rb, STP065-12/Sb, STP085-12/Bb." Retrieved September 20, 2016, from http://www.fibat.ro/energie_neconv/panouri_ibc_solar/6.pdf.